# Dimensional Synthesis of the

# Single-Loop Translational Parallel Manipulator PRRR-PRPU

**Raffaele Di Gregorio** (*)
Department of Engineering, University of Ferrara
Via Saragat,1; 44122 FERRARA; Italy
T: +39-0532-974828, F: +39-0532-974870
E: raffaele.digregorio@unife.it

**Henrique Simas**
Raul Guenther Lab. of Applied Robotics - Department of Mechanical Engineering
Federal University of Santa Catarina
Florianópolis, SC- Brazil - 88040-900
E: henrique.simas@ufsc.br

(*) Corresponding author

**Abstract:** The dimensional synthesis of translational parallel manipulators (TPMs) of type PRRR-PRPU is addressed by using an overall novel method. Addressing this design step on such TPMs is interesting for the scientific community since, in a previous paper, one of the authors showed that it has the following promising features: a single-loop not-overconstrained architecture with all the actuators on or near to the base, a simple position analysis, easy-to-find workspace boundaries, no constraint singularity, a type-II singularity locus that is a plane easy to keep far from the useful workspace, and a double infinity of isotropic configurations. The presented synthesis includes the analysis of isotropy and dexterity by local and global conditioning indexes, the useful workspace optimization, and the accuracy and stiffness analyses. The result is the identification of a normalized TPM of type PRRR-PRPU with performances that are comparable with those of commercial TPMs. The identified normalized TPM yields a set of actual TPMs with the same performances by changing the value of a reference geometric length. Also, the chosen shape of the useful workspace (i.e., a cuboid) matches the needs of many industrial applications.

**Keywords:** translational parallel manipulators, dimensional synthesis, kinetostatic performances, stiffness, positioning precision

## 1. Introduction

A great number of TPMs have been proposed in the literature (see, for instance, [1-6]). Most of them feature three kinematic chains (limbs) with equal topology, which join the end effector (platform) to the frame (base), and one actuated joint per limb. Their type synthesis mainly relies either on the screw theory (e.g., [1]) or on the intersection of displacement sub-groups [2]. The first approach looks for limbs whose passive structures (i.e., without actuators)

apply to the platform only one torque, and use three of such limbs in an arrangement that makes them apply three non-coplanar torques to the platform. This approach identifies limbs with connectivity[1] 5. The second approach looks for limbs (mechanical generators) that generate Shoenflies motions[2] [8] and combines three of them [2, 9] so that the rotation axes of the Shoenflies motion generated by at least two limbs are not parallel. This approach identifies limbs with connectivity 4 and overconstrained architectures that can become not-overconstrained by adding idle passive pairs; also, it highlights that two limbs, that is, a single-loop architecture, are sufficient to obtain a TPM.

In this context, one of the authors [11] has recently highlighted that, according to Chebychev-Grübler-Kutzbach formula and Euler's formula [10], the combination of one limb with connectivity 4, which constrains the platform to a Shoenflies motion, and another limb with connectivity 5, whose passive structure applies to the platform only one torque with a component parallel to the rotation axis of that Shoenflies motion, yields a single-loop not-overconstrained architecture where the platform can only perform spatial translations (i.e., a TPM architecture). In short, any limb identified through the second approach when suitably combined with any limb identified through the first approach yields a single-loop not-overconstrained TPM architecture.

This "novel" type synthesis technique generates a family of TPMs that, in general, have simplified architectures, and whose manufacturing does not need small dimensional tolerances since they are not-overconstrained. Also, such architectures allow the introduction of two actuators on the base and of the remaining one near to the base, which should not drastically reduce the dynamic performances with respect to three-limbed architectures with all the actuators on the base.

The TPM architecture of type PRRR-PRPU[3] shown in Fig. 1 belongs to this family. In [11], such architecture was proved to have the following qualities, relevant from the design point of view: (i) two simple explicit formulas solve its position analysis problems, (ii) its workspace boundaries are easy to find, (iii) it has no constraint singularity [12], (iv) its type-II singularity locus [13-15] is a plane easy to keep far from the useful workspace, and (v) it has a double infinity of isotropic configurations [16, 17]. Nevertheless, only the dimensional synthesis of TPMs of type PRRR-PRPU can fully reveal their potentialities. Such design step has not been addressed, yet, in the literature. This paper fills this gap.

[1] The term "connectivity" [7] referred to two links of a mechanism indicates the number of degrees-of-freedom (dof) of the relative motion between those two links. Here, the phrase "limb connectivity" stands for the connectivity between platform and base when connected only by that limb.

[2] The displacement sub-groups of Shoenflies, $\{X(\mathbf{u})\}$, are the unions of the spatial translation sub-group, $\{T\}$, with one rotation-around-an-axis sub-group, $\{R(C,\mathbf{u})\}$, where $\mathbf{u}$ and C are the unit vector and a point of the rotation axis. Since the unit vectors are $\infty^2$, as many are the Shoenflies sub-groups.

[3] P, R and U stand for prismatic pair, revolute pair and universal joint, respectively. The underscores indicate the actuated pairs; whereas, the hyphen separates the strings which give the limb topologies by moving from the base to platform.

Here, a detailed dimensional synthesis of TPMs of type PRRR-PRPU is presented and discussed. The adopted synthesis method is overall novel and can be used for the dimensional synthesis of any TPM. It includes the isotropy and dexterity analyses by local and global conditioning indexes, the useful workspace optimization, and the accuracy and stiffness analyses. The result of the presented dimensional synthesis is the identification of a normalized TPM of type PRRR-PRPU with performances that are comparable with those of commercial TPMs. The identified normalized TPM yields a set of actual TPMs with the same performances by changing the value of a reference geometric length.

The paper is organized as follows. Section 2 presents the PRRR-PRPU architecture and the used notations; then, briefly summarizes the results obtained in [11]. Section 3 addresses the dimensional synthesis of the PRRR-PRPU architecture by taking into account its kinetostatic performances, its overall size and its stiffness. Section 4 presents the accuracy analysis of the architecture with the size ratios determined in section 3. Eventually, section 5 discusses the results and draws the conclusions.

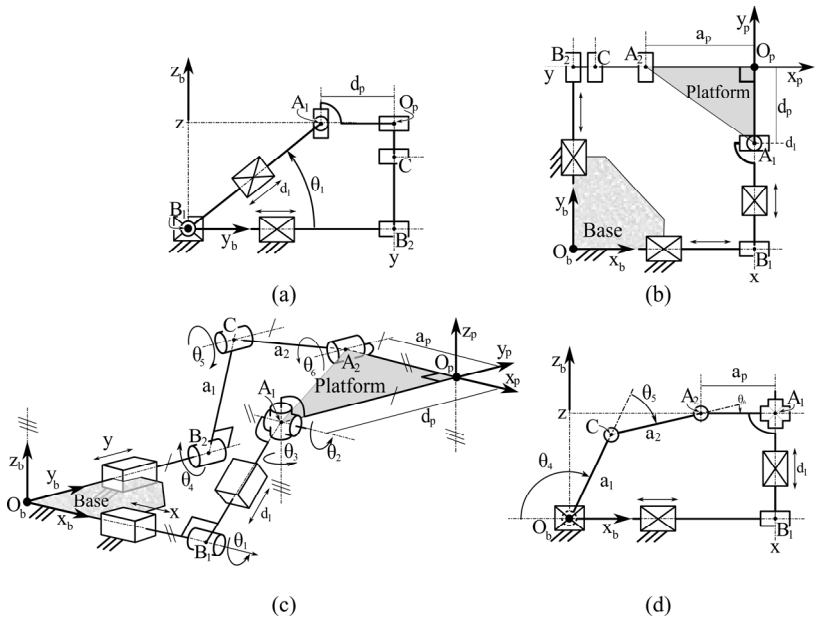


**Figure 1:** The TPM architecture of type PRRR-PRPU: (a) $y_bz_b$-plane view, (b) $x_by_b$-plane view, (c) 3D view (b) $x_bz_b$-plane view

## 2. The TPM of Type PRRR-PRPU: Notations and Background

Figure 1 shows the PRRR-PRPU architecture presented in [11]. The PRRR limb is the mechanical generator of Shoenflies displacements. In this limb, the P-pair sliding direction and the three R-pair axes are all parallel to the

$y_b$ axis of the Cartesian reference $O_b$–$x_by_bz_b$, fixed to the base; consequently, this coordinate axis has the direction of the rotation axis of the generated Shoenflies motion. The passive structure of the PRPU limb applies to the platform only one torque perpendicular to the cross link of the U-joint. This torque has a direction that does not change during motion and is parallel to the $y_b$ axis. Indeed, the PRPU limb is so sized that the axes of the two intermediate R pairs are parallel to each other and are constrained to translate with respect to the base by keeping the direction of the $x_b$ axis; whereas, the axis of the third R pair is perpendicular to those of the two intermediate and is fixed to the platform that keeps it perpendicular to the $y_b$ axis, too.

With reference to Fig. 1, $A_1$ is the center of the U joint. $O_p$ is the platform reference point whose coordinates, $(x, y, z)^T$, measured in $O_b$–$x_by_bz_b$ will be used to identify the platform pose (the platform can only translate with respect to the base). $A_2$ is the foot of the perpendicular from $O_p$ to the axis of the R pair that joins the platform to the PRRR limb. $O_p$, $A_1$, and $A_2$ are the vertices of a right triangle, fixed to the platform, which lies on a plane parallel to the $x_by_b$ coordinate plane. $a_p$ and $d_p$ are the lengths of the segments $O_pA_2$ and $O_pA_1$, respectively. $B_1$ is the foot of the perpendicular from $A_1$ to the axis of the R pair between the two actuated P pairs of the PRPU limb, and $d_1$ is the length of the segment $A_1B_1$. $B_2$ and C are the feet of the perpendiculars from $A_2$ to the axes of the two intermediate R pairs of the PRRR limb; whereas, $a_1$ and $a_2$ are the lengths of the segments $B_2C$ and $CA_2$, respectively. Hereafter, $\mathbf{i}_b$, $\mathbf{j}_b$, and $\mathbf{k}_b$ will denote the unit vectors of the coordinate axes $x_b$, $y_b$, and $z_b$, respectively.

The x and y coordinates of $O_p$ coincides with the actuated joint variables of the two P pairs adjacent to the base [see Fig. 1(b)]; whereas, the third actuated joint variable, $d_1$, can be explicitly expressed as a function of the $O_p$ coordinates as follows [see Fig. 1(c)]

$$d_1 = \sqrt{(y - d_p)^2 + z^2} \tag{1}$$

which also yields

$$z = \pm\sqrt{d_1^2 - (y - d_p)^2} \tag{2}$$

If the $O_p$ coordinates, x, y, and z, are assigned (Inverse Position Analysis (IPA)), the actuated-joint variables, x, y, and $d_1$, are determined uniquely and straightforwardly with Eq. (1). Conversely, if the actuated-joint variables are assigned (Direct Position Analysis (DPA)), the $O_p$ coordinates can assume two set of values which share the same x and y values, but have the opposite z values given by Eq. (2). These two solutions of the DPA yield a workspace symmetric with respect to the $x_by_b$ coordinate plane.

The workspace, represented by using the $O_p$ coordinates as coordinates of the operational space, is the intersection volume of two right circular cylindrical shells. One is due to the PRPU limb and has the axis parallel to the $x_b$ axis and passing through the point $(0, d_p, 0)^T$, and the inner and outer radii equal to the minimum and

maximum values of $d_1$. The other is due to the PRRR limb and has the axis parallel to the $y_b$ axis and passing through the point $(a_p, 0, 0)^T$, and the inner and outer radii equal to $|a_1 - a_2|$ and $(a_1 + a_2)$, respectively.

One of these authors [11] demonstrated that this TPM has no constraint singularity[4] and deduced its input-output instantaneous relationship as follows:

$$\dot{\mathbf{O}}_p = \dot{x}\,\mathbf{i}_b + \dot{y}\left(\mathbf{j}_b - \frac{\cos\theta_1}{\sin\theta_1}\mathbf{k}_b\right) + \dot{d}_1\left(\frac{1}{\sin\theta_1}\mathbf{k}_b\right) \tag{3}$$

Since the x and y coordinates of $O_p$ are also actuated-joint variables, singularities[5] may occur only in the relationship between $\dot{z}$ and the actuated joints' rates, $\dot{x}$, $\dot{y}$, and $\dot{d}_1$. Actually, after a simple expansion, Eq. (3) reduces itself to two identities plus the following scalar equation

$$\dot{z}\sin\theta_1 = \dot{d}_1 - \dot{y}\cos\theta_1 \tag{4}$$

Thus, type-II singularities occur when $\theta_1$ is equal to zero, that is, when $O_p$ lies on the plane z=0 [see Fig. 1(a)]; whereas, no type-I singularities are present. Also, Eq. (4) and Fig.1(a) highlight that, when $O_p$ lies on the plane $y=d_p$, $\theta_1$ is equal to ±90° and the Jacobian matrix that relates the platform translation velocity, $\dot{\mathbf{O}}_p$, to the actuated joints' rates, $\dot{x}$, $\dot{y}$, and $\dot{d}_1$ is equal to **diag**(1,1,±1); hence, at these configurations, it has all its singular values equal to one. The configurations where the singular values of this Jacobian are all equal and non-null are named isotropic [16, 17] and provide the best kinetostatics performances. Therefore, this TPM is an isotropic manipulator[6] that can reach $\infty^2$ isotropic configurations corresponding to the points of the plane $y=d_p$. Locating its useful workspace around the plane $y=d_p$ yields the best kinetostatics design.

## 3. Dimensional Synthesis

The determination of the actual sizes (dimensional synthesis) of a manipulator is mainly related [16, 18-20] to the design requirements on the kinetostatics performances and the ratio (volumetric ratio) between its useful workspace and its overall size. Once the manipulator geometry has been defined, stiffness and accuracy analyses are always necessary to evaluate the quality of the designed machine [21-23].

[4] In TPMs, constraint singularities are configurations where the angular velocity of the platform can be different from zero [12].

[5] Singularities [13-15] are manipulator's configurations where the instantaneous input-output relationship fails to state a one-to-one correspondence between instantaneous inputs (i.e., the actuated joints' rates) and outputs (i.e., the platform twist). Type-I (serial) singularities occurs when the actuated joints' rates are not determined even though the platform twist is assigned; vice versa, type-II (parallel) singularities occurs when the platform twist is not determined even though the actuated joints' rates are assigned; eventually, type-III singularities are configurations where both the two previous conditions are satisfied.

[6] The manipulators that can reach one or more isotropic configurations are named isotropic [16, 17].

In this section, first of all the useful workspace will be identified by fixing the minimum local kinetostatics performances; then, the actual sizes will be determined by maximizing the volumetric ratio and, eventually, the stiffness analysis of the defined geometry will be presented. Since the design requirements on kinetostatics performances are not sufficient to fully define the links' geometry, this design procedure will be implemented by assuming that the ratios between the sizes of some geometric parameters (see Fig. 1) have the following values (l.u. stands for length unit):

- the stroke, $\Delta d_1 = d_{1max} - d_{1min}$ , of the actuated-joint variable $d_1$ is equal to 1 (l.u.);

- the minimum value, $d_{1min}$, of the actuated-joint variable $d_1$ is equal to 0.3 (l.u.);

- the sum $(a_1+a_2)$ is equal to 1.31 (l.u.);

- the platform parameters $a_p$ and $d_p$ are both equal to 0.12 (l.u.).

Such normalized values have been determined to have a well-proportioned manipulator and by checking similar dimensions of some commercial TPMs.

**3.1 Local and Global Kinetostatics Performances:**

Kinetostatics performances increase with the "distance" from singular configurations[5]. In the literature [16, 20, 24-28], such "distance" is evaluated with the "Conditioning Index" (CI). In parallel manipulators, the CI is defined as the inverse of the condition number of the Jacobian matrix, hereafter named **H**, whose product by the platform twist (i.e., $\dot{\mathbf{O}}_p$ for the studied TPM) yields the vector of the actuated-joint rates [i.e., $\dot{\mathbf{q}}_f = (\dot{x}, \dot{y}, \dot{d}_1)^T$ in the case under study]. It ranges from 0, at singular configurations, to 1, at isotropic configurations, which are the best configurations. If the spectral norm [29] is adopted to compute the condition number, the so-defined CI is equal to the ratio between the smallest and the largest singular values of **H**. Equations (3) and (4) with simple algebraic manipulations give the following analytic expression of **H** for the studied TPM:

$$\mathbf{H} = \begin{bmatrix} 1 & 0 & 0 \\ 0 & 1 & 0 \\ 0 & \cos\theta_1 & \sin\theta_1 \end{bmatrix} \tag{5}$$

Equation (5) yields

$$CI = \sqrt{\frac{1-|\cos\theta_1|}{1+|\cos\theta_1|}} \tag{6}$$

where $|(\cdot)|$ denotes the absolute value of $(\cdot)$.

Locating the useful workspace in the region of the operational workspace where the CI is greater than or equal to a given value, $CI_{min}$, is the usual way to guarantee that the kinetostatics performances are good enough. In the studied case, the inequality $CI \geq CI_{min}$, together with Eq. (6) yields

$$\left|\cos\theta_1\right| \le \frac{1-\mathrm{CI}_{\min}^2}{1+\mathrm{CI}_{\min}^2} \tag{7}$$

which gives the geometric condition $\varphi \le \left|\theta_1\right| \le \pi - \varphi$ where $\theta_1 \in ]-\pi, +\pi]$ and

$$\varphi = \cos^{-1}\left(\frac{1-\mathrm{CI}_{\min}^2}{1+\mathrm{CI}_{\min}^2}\right) \tag{8}$$

The region of the operational workspace that satisfies inequality (7) and is located in the half-space $z \ge 0$ is shown in Fig. 2; since the operational workspace (see section 2) of the studied TPM is symmetric with respect to the plane z=0, which is also the geometric locus of all the type-II singularities, the workspace region, located in the half-space $z \le 0$ and symmetric with respect to the plane z=0, also satisfies the same inequality. Since these two regions are not connected and are separated by the singularity plane z=0, the useful workspace must be located in only one of them. Hereafter, the half-space $z \ge 0$ is chosen to locate the useful workspace; also, $\mathrm{CI}_{\min}$ is chosen equal to 0.63 when its value is necessary to define the geometry of the TPM. Equation (8) gives $\varphi$ = 1.12 rad for $\mathrm{CI}_{\min}$=0.63. Figure 3 shows the diagram of CI (Eq.(6)) as a function of $\theta_1$ for $\theta_1 \in [\varphi, \pi-\varphi]$ rad with $\varphi$ = 1.12 rad.

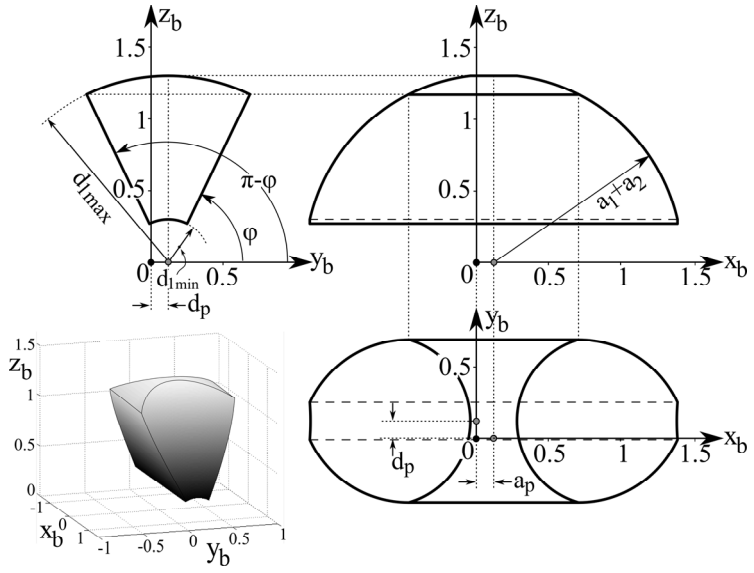


**Figure 2**: Region of the operational workspace that satisfies inequality (7) and is located in the half-space $z \ge 0$ ($\varphi$= 1.12 rad, if $\mathrm{CI}_{\min}$=0.63). The values reported on the coordinate axes refer to the following assigned data: $a_1+a_2$=1.31(l.u.), $a_p$=0.12(l.u.), $d_p$=0.12(l.u.), $d_{1\min}$=0.3(l.u.), and $d_{1\max}$=1.3(l.u.).

The useful workspace is a regular geometric object (e.g., a cube or a ball in a 3-dof case) [30, 31] located in the region of the operational workspace that satisfies all the kinetostatics requirements. In the studied case, its shape is chosen equal to a rectangular parallelepiped, whose edges have more or less the same length, that is located in the workspace region shown in Fig. 2, with $\varphi$ = 1.12 rad, and touches the boundaries of this region. Figure 4 shows the definition of the parameter $y_a$ and the projections into the $y_bz_b$-coordinate plane of the useful workspace, $A_{yz}$, and of

the operational workspace region, $W_{yz}$. With reference to Fig. 4, the volume, $V_u$, of such parallelepiped has been expressed as a function of the parameter $y_a$, and the value of $y_a$ that maximizes $A_{yz}$ has been determined in order to find the best solution. The $A_{yz}$ area as a function of $y_a$ is

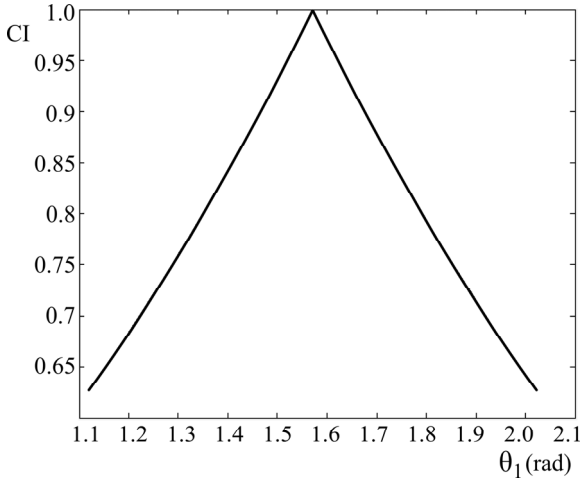


**Figure 3**: Diagram of CI (Eq.(6)) as a function of $\theta_1$ for $\theta_1 \in [\varphi, \pi-\varphi]$ rad with $\varphi = 1.12$ rad.

$$A_{yz}(y_a)=2(y_a-d_p)\left(\sqrt{d_{1max}^2-(y_a-d_p)^2}-(y_a-d_p)\tan\varphi\right) \tag{9}$$

whose derivative with respect to $y_a$, when equated to zero, yields the following value, $y_{a,lim}$, for $y_a$

$$y_{a,lim}=d_p \pm d_{1max}\sqrt{\frac{\sqrt{(1+\tan^2\varphi)}-\tan\varphi}{2\sqrt{(1+\tan^2\varphi)}}}=d_p \pm y_p \tag{10}$$

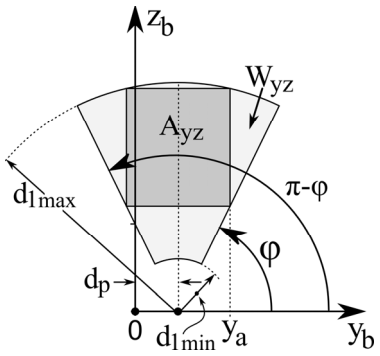


**Figure 4**: The projections into the $y_bz_b$-coordinate plane of the useful workspace, $A_{yz}$, and of the operational workspace region, $W_{yz}$, and the definition of $y_a$.

The introduction of expression (10) into the other relationships that define $V_u$ yields the values reported in Tables 1 and 2, and the $V_u$ shown in Fig. 5.

The CI evaluates the local kinetostatics performance of a manipulator at a given configuration. Based on the CI, the global conditioning index (GCI), defined as the average CI value on $V_u$, has been proposed [16] to score the complete kinetostatics performances of a manipulator. In the studied TPM, the relationship (see Fig. 1)

$$|\cos\theta_1| = \frac{|y - d_p|}{\sqrt{z^2 + (y - d_p)^2}}, \tag{11}$$

**Table 1**: Coordinates of $V_u$ parallelepiped's vertices (φ=1.12rad)

| | | |
|---|---|---|
| $x_{min}$ | –0.21243 (l.u.) | $x_{min} = a_p - \sqrt{(a_1+a_2)^2 - z_{max}^2}$ |
| $x_{max}$ | 0.45243 (l.u.) | $x_{max} = a_p + \sqrt{(a_1+a_2)^2 - z_{max}^2}$ |
| $y_{min}$ | –0.17054 (l.u.) | $y_{min} = d_p - y_p$ |
| $y_{max}$ | 0.41054 (l.u.) | $y_{max} = d_p + y_p$ |
| $z_{min}$ | 0.60025 (l.u.) | $z_{min} = (y_{max} - d_p)\tan\varphi$ |
| $z_{max}$ | 1.26712 (l.u.) | $z_{max} = \sqrt{d_{1max}^2 - (y_{max} - d_p)^2}$ |

**Table 2**: Sections' areas and volume of $V_u$ for φ=1.12rad

| | |
|---|---|
| $A_{xy}$ | 0.38634 (l.u.)$^2$ |
| $A_{xz}$ | 0.44338 (l.u.)$^2$ |
| $A_{yz}$ | 0.38751 (l.u.)$^2$ |
| $V_u$ volume | 0.25764 (l.u.)$^3$ |

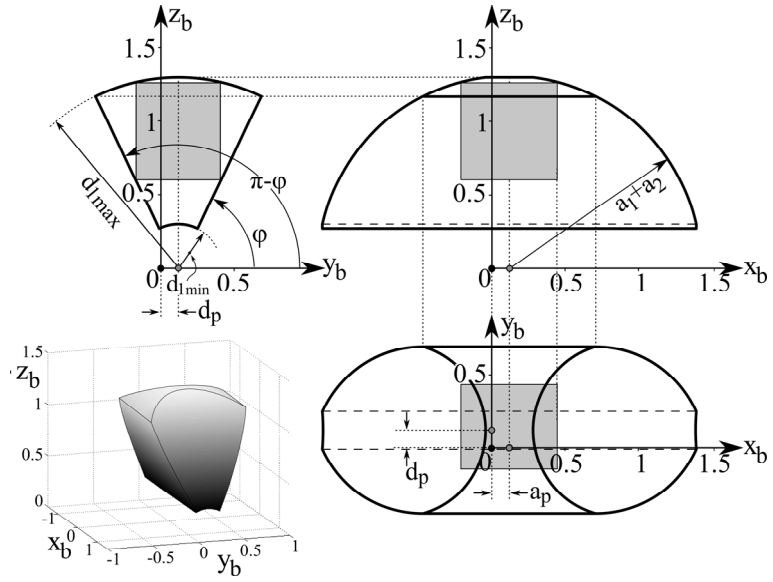


**Figure 5**: Useful workspace $V_u$: $a_1+a_2$=1.31(l.u.), $a_p$=0.12(l.u.), $d_p$=0.12(l.u.), $d_{1min}$=0.3(l.u.), $d_{1max}$=1.3(l.u.), and CI≥0.63

when introduced into Eq. (6), yields the following GCI expression

$$GCI = \frac{\iiint_{V_u} \sqrt{\frac{\sqrt{z^2 + (y-d_p)^2} - |y-d_p|}{\sqrt{z^2 + (y-d_p)^2} + |y-d_p|}}\, dxdydz}{\iiint_{V_u} dxdydz} \equiv \frac{\iint_{A_{yz}} \sqrt{\frac{\sqrt{z^2 + (y-d_p)^2} - |y-d_p|}{\sqrt{z^2 + (y-d_p)^2} + |y-d_p|}}\, dydz}{(y_{max} - y_{min})(z_{max} - z_{min})} \tag{12}$$

The introduction of the values of Table 1 into Eq. (12) yields GCI=0.855. This GCI value has been computed with an iterative numerical algorithm that, at the k-th iteration, uses the formula

$$GCI_k = \frac{1}{n_k m_k} \sum_{\substack{i=1,n_k \\ j=1,m_k}} \sqrt{\frac{\sqrt{z_j^2 + (y_i - d_p)^2} - |y_i - d_p|}{\sqrt{z_j^2 + (y_i - d_p)^2} + |y_i - d_p|}}, \tag{13}$$

where $z_j=z_{min}+(j-1)\Delta_k$, $y_j=y_{min}+(i-1)\Delta_k$, $n_k=INT[(y_{max}-y_{min})/\Delta_k]$,[7] and $m_k=INT[(z_{max}-z_{min})/\Delta_k]$ with $\Delta_1=(y_{max}-y_{min})/2000$ and $\Delta_k=\Delta_{k-1}/2$. The algorithm stops the iteration if $|GCI_k - GCI_{k-1}|\leq 10^{-4}$.

**3.2 Volumetric Ratio:**

The ratio (volumetric ratio), $r_V$, between the volume of the useful workspace (hereafter, referred to as $V_u$ for the sake of simplicity) and the volume (overall size), $V_o$, that encloses all the TPM's links during its motion is an important installation parameter that is always provided by the manipulators' data sheets. At parity of $V_u$, the higher $r_V$ is, the better the geometric dimensioning of the machine is. Thus, maximizing $r_V$ is a task to undertake during the design of the machine.

For the studied TPM, $V_o$ has been identified through a mobility analysis implemented in GeoGebra[8] by using its 3D graphic tools. Figure 6 shows the projections onto the coordinate planes of one determination of $V_o$ together with one TPM configuration corresponding to a set of assigned values of the actuated-joint variables. $V_o$ varies as a function of the actual sizes of the links. According to the previously assigned geometric data only the lengths $a_1$ and $a_2$ (see Fig. 1) can be changed provided that the constraint $a_1+a_2 = 1.31$(l.u.) is satisfied. In order to find the maximum value of $r_V$, the positions $a_1=1.31(1-k_a)$ and $a_2=1.31k_a$, where $k_a$ is a parameter varying from 0 to 1, have been introduced; then, for each value of $k_a$, $V_o$ has been determined as above explained and $r_V$ ($=V_u/V_o$) has been computed. The diagram shown in Fig. 7 is the result of this computation.

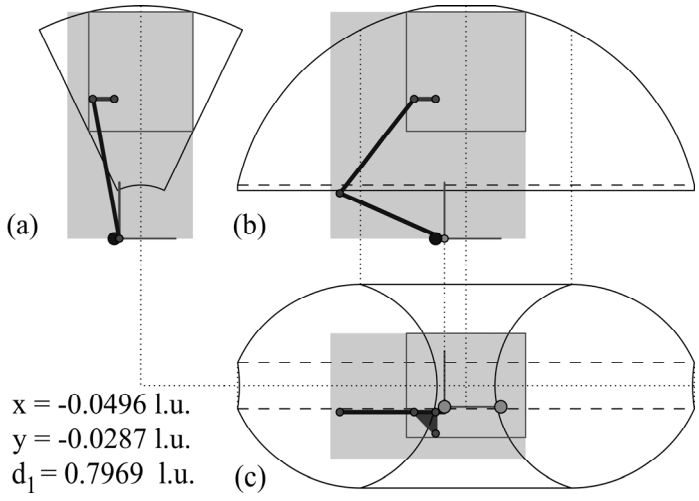


**Figure 6:** One determination of $V_o$: the gray rectangles are the projections of $V_o$ onto (a) the $y_bz_b$-plane, (b) the $x_bz_b$-plane, and (c) the $x_by_b$-plane

[7] INT[(·)] stands for integer part of (·).
[8] GeoGebra is a freely dowloadable (https://www.geogebra.org/) software mainly conceived to teach mathematics.

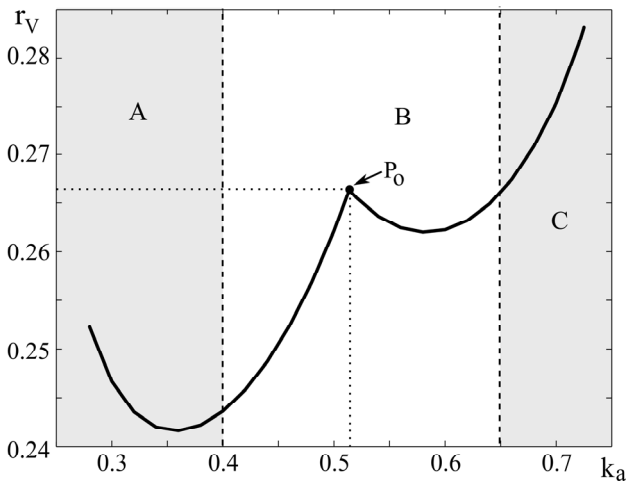


**Figure 7:** Diagram of $r_V$ as a function of the parameter $k_a$.

In the diagram of Fig. 7, the values of $r_V$ for $k_a<0.4$ (area A) correspond to PRPU-PRRR architectures whose links invaded the useful workspace during the mobility analysis; whereas, the values of $r_V$ for $k_a>0.65$ (area C) correspond to PRPU-PRRR architectures whose links, during the mobility analysis, invaded the half-space $z<0$ and reached configurations where the transmission angle [$=\pi - \theta_5$ (see Fig. 1(d))] between the two links of the RRR dyad of the PRRR limb is too small[9]. Thus, only the values of $r_V$ for $0.4<k_a<0.65$ (area B) are acceptable and, in this range, the maximum value of $r_V$ corresponds to point $P_0$ of Fig. 7 where $r_V=0.266$[10] and $k_a=0.514$. These values yield $a_1=0.637$ (l.u.), $a_2=0.673$ (l.u.), $V_o=0.9678$ (l.u.)$^3$, the values of Table 3 and the $V_o$ shown in Fig. 8.

**Table 3**: Coordinates of $V_o$ parallelepiped's vertices ($x_{max}$, $y_{min}$, $y_{max}$, and $z_{max}$ are reported in Table 1)

| | | |
|---|---|---|
| $X_{min}$ | –0.637 (l.u.) | $X_{min}=-a_1$ |
| $X_{max}$ | 0.45243 (l.u.) | $X_{max}=x_{max}$ |
| $Y_{min}$ | –0.29054 (l.u.) | $Y_{min}=y_{min}-d_p$ |
| $Y_{max}$ | 0.41054 (l.u.) | $Y_{max}=y_{max}$ |
| $Z_{min}$ | 0 (l.u.) | |
| $Z_{max}$ | 1.267083 l.u | $Z_{max}=z_{max}$ |

[9] In the literature (see [32], for instance) a transmission angle lower than 45° is considered too near to the fully folded (singular) configuration of the RRR dyad.

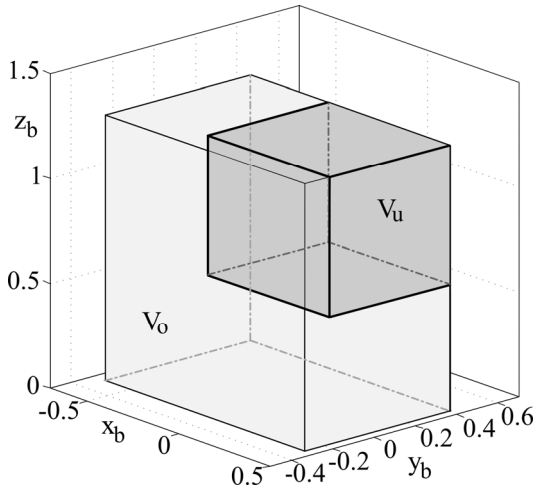


**Figure 8**: $V_u$ and $V_o$ corresponding to $r_V$=0.266.

**3.3 Stiffness Analysis:**

The stiffness analysis [21, 33-35] of not-overconstrained manipulators usually assumes that only the actuated joints are flexible in the structure generated by locking the actuators. Here, this hypothesis yields the following relationship:

$$\boldsymbol{\tau} = \mathrm{diag}(\mathbf{k})\Delta\mathbf{q}_f \tag{14}$$

where $\Delta\mathbf{q}_f = (\Delta x, \Delta y, \Delta d_1)^T$ collects the variations of the actuated-joint variables; whereas, $\boldsymbol{\tau} = (\tau_x, \tau_y, \tau_d)^T$ and $\mathbf{k} = (k_x, k_y, k_d)^T$ collect the generalized forces applied by the actuators and the stiffness of the actuated joints, respectively, of the three actuated P pairs (the right subscripts, x, y and d, identify the P pairs with their joint variables, that is, x, y, and $d_1$).

Also, the application of the virtual work principle to the studied TPM, by taking into account the relationship $\dot{\mathbf{q}}_f = \mathbf{H}\dot{\mathbf{O}}_p$, yields the following static relationships

$$\mathbf{f} = \mathbf{H}^T\boldsymbol{\tau} \tag{15}$$

where $\mathbf{f}=(f_x,f_y,f_z)^T$ is the resultant force, measured in $O_b$–$x_by_bz_b$, of the force system the platform applies when interacting and Eq. (5) gives the explicit expression the Jacobian matrix **H**; whereas, if the small finite variations

[10] The published data (http://new.abb.com/products/robotics/industrial-robots/irb-360) of the commercial delta robot ABB IRB-360 bring to compute $r_V$=0.253 for the ABB IRB-360.

$\Delta\mathbf{q}_f$ and $\Delta\mathbf{O}_p$ [=$(\Delta x, \Delta y, \Delta z)^T$] replace (1st order approximation) $\dot{\mathbf{q}}_f$ and $\dot{\mathbf{O}}_p$, respectively, into $\dot{\mathbf{q}}_f = \mathbf{H}\dot{\mathbf{O}}_p$ the following relationship will result

$$\Delta\mathbf{q}_f = \mathbf{H}\,\Delta\mathbf{O}_p \tag{16}$$

The introduction of expression (16) into Eq. (14) and of the resulting expression into Eq. (15) yields

$$\mathbf{f} = \mathbf{H}^T \text{diag}(\mathbf{k})\,\mathbf{H}\,\Delta\mathbf{O}_p = \mathbf{K}_s\,\Delta\mathbf{O}_p \tag{17}$$

where the stiffness matrix $\mathbf{K}_s$ [=$\mathbf{H}^T$ diag($\mathbf{k}$) $\mathbf{H}$] has the following explicit expression

$$\mathbf{K}_s = \begin{bmatrix} k_x & 0 & 0 \\ 0 & k_y + k_d(\cos\theta_1)^2 & k_d\cos\theta_1\sin\theta_1 \\ 0 & k_d\cos\theta_1\sin\theta_1 & k_d(\sin\theta_1)^2 \end{bmatrix} \tag{18}$$

The square root of the ratio between the smallest and the largest eigenvalues of the stiffness matrix [21] is an index, ($1/k_s$), ranging from 0 to 1, that measures the stiffness isotropy and coincides with the CI of the Jacobian matrix $\mathbf{H}$ [i.e., Eq. (6)] when $k_x=k_y=k_d$ . The eigenvalues of $\mathbf{K}_s$ have the following explicit expressions:

$$\lambda_1 = k_x, \quad \lambda_{2,3} = \frac{1}{2}\left(k_y + k_d \mp \sqrt{k_y^2 + k_d^2 + 2k_y k_d\cos(2\theta_1)}\right) \tag{19}$$

According to Eq. (19), the values of the ratios between $k_x$, $k_y$, and $k_d$ determine which $\lambda_i$, for i=1,2,3, is the smallest or the largest. In general, the linear actuators of the two P pairs on the base can be of the same type, which implies $k_x=k_y$; whereas, the linear actuator of the remaining P pair, which controls the joint variable $d_1$, must match different technical requirements and could be different from the other two with $k_d=c_k\,k_x$ where $c_k$ is a constant parameter greater than 0. In this case, Eq. (19) allows the identification of the smallest and the largest $\lambda_i$, i=1,2,3, and gives the following explicit expression of $1/k_s$

$$\frac{1}{k_s} = \sqrt{\frac{1+c_k - \sqrt{1+c_k^2+2c_k\cos(2\theta_1)}}{1+c_k+\sqrt{1+c_k^2+2c_k\cos(2\theta_1)}}} \tag{20}$$

Figure 9 shows the 3D diagram of expression (20) as a function of $c_k$, for $c_k \in ]0, 3]$, and $\theta_1$, for $\theta_1 \in ]\varphi, \pi-\varphi]$ rad with $\varphi$=1.12 rad. The intersection of this diagram with the plane $c_k$=1, which corresponds to $k_x=k_y=k_d$, coincides with the diagram of the CI (i.e., Eq. (6) and Fig. 3) as a function of $\theta_1$. Also, since the derivative with respect to $c_k$ of expression (20) is always equal to zero when $c_k$=1, this intersection (i.e., the CI as a function of $\theta_1$ given by Eq.(6) and Fig. 3) gives the maximum value of $1/k_s$ as a function of $\theta_1$. The conclusion is that, from the point of view of the stiffness isotropy, the best design is obtained by choosing all the actuators of the same type (i.e., $k_x=k_y=k_d$). This goal could be obtained by using rollerball linear actuators, which join high stiffness to the possibility of being mounted on P pairs both adjacent and not-adjacent to the base.

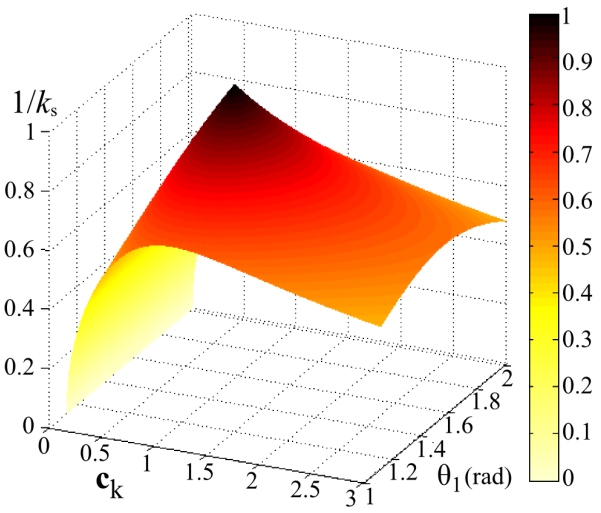


**Figure 9**: 3D diagram of expression (20) as a function of $c_k$, for $c_k \in ]0, 3]$, and $\theta_1$, for $\theta_1 \in ]\varphi, \pi-\varphi]$ rad with $\varphi$=1.12 rad.

## 4. Accuracy Analysis

Accuracy analysis determines the positioning precision of a manipulator when manufacturing and/or assembly errors (geometric errors) are present and relates geometric tolerances to the positioning precision requirements. This analysis is necessary for lower-mobility manipulators (e.g., TPMs) [22, 23, 36] since their calibration procedures cannot compensate the effects of the geometric errors that make the platform perform motions which do not belong to the displacement sub-group (e.g., the spatial translation sub-group {T} for TPMs) the platform is designed to move in.

These authors presented a general technique to perform the accuracy analysis in a previous paper [23]. Such technique will be used in this section. It consists in

(a) the identification of the "independent geometric constants (IGCs)" that define the geometry of the links,

(b) the generation of an "Extended Spatial Mechanism (ESM)" which contains only P and/or R pairs and is obtained from the actual manipulator by considering as additional passive-joint variables the IGCs whose changes make the platform move out of its nominal displacement sub-group,

(c) the determination of the following form of the instantaneous input-output relationship of the ESM ($\boldsymbol{\omega}$ is the angular velocity of the platform)

$$\boldsymbol{\omega} = \mathbf{D}_{f,P}\ \dot{\mathbf{q}}_{f,P} + \mathbf{D}_{f,R}\ \dot{\mathbf{q}}_{f,R} + \mathbf{D}_{g,P}\ \dot{\mathbf{q}}_{g,P} + \mathbf{D}_{g,R}\ \dot{\mathbf{q}}_{g,R} \tag{21a}$$

$$\dot{\mathbf{O}}_p = \mathbf{E}_{f,P}\ \dot{\mathbf{q}}_{f,P} + \mathbf{E}_{f,R}\ \dot{\mathbf{q}}_{f,R} + \mathbf{E}_{g,P}\ \dot{\mathbf{q}}_{g,P} + \mathbf{E}_{g,R}\ \dot{\mathbf{q}}_{g,R} \tag{21b}$$

where $\mathbf{q}_{f,P}$ and $\mathbf{q}_{f,R}$ ($\mathbf{q}_{g,P}$ and $\mathbf{q}_{g,R}$) collect all the joint variables of P and R pairs, respectively, that appear among the actuated-joint variables (among the additional passive-joint variables obtained from the IGCs),

(d) the computation of the coefficients that appear in the following relationship [see [23] for the deduction from Eq. (21)] between the errors on the platform pose and the geometric errors[11]

$$|\Delta\varphi| \leq \delta_{f,P} \, ||\Delta\mathbf{q}_{f,P}|| + \delta_{f,R} \, ||\Delta\mathbf{q}_{f,R}|| + \delta_{g,P} \, ||\Delta\mathbf{q}_{g,P}|| + \delta_{g,R} \, ||\Delta\mathbf{q}_{g,R}|| \tag{22a}$$

$$||\Delta\mathbf{O}_p|| \leq \varepsilon_{f,P} \, ||\Delta\mathbf{q}_{f,P}|| + \varepsilon_{f,R} \, ||\Delta\mathbf{q}_{f,R}|| + \varepsilon_{g,P} \, ||\Delta\mathbf{q}_{g,P}|| + \varepsilon_{g,R} \, ||\Delta\mathbf{q}_{g,R}|| \tag{22b}$$

where $\delta_{f,P}$ , $\delta_{f,R}$ , $\delta_{g,P}$ , $\delta_{g,R}$ , $\varepsilon_{f,P}$ , $\varepsilon_{f,R}$ , $\varepsilon_{g,P}$ , and $\varepsilon_{g,R}$, named "accuracy coefficients", are the largest singular values of the Jacobian matrices $\mathbf{D}_{f,P}$ , $\mathbf{D}_{f,R}$ , $\mathbf{D}_{g,P}$ , $\mathbf{D}_{g,R}$ , $\mathbf{E}_{f,P}$ , $\mathbf{E}_{f,R}$ , $\mathbf{E}_{g,P}$ , and $\mathbf{E}_{g,R}$, respectively, and $\Delta\varphi$ is the rotation angle of the rotation matrix that represents the rotation which makes the nominal platform orientation coincide with the actual one (i.e., the one that takes into account the orientation error).

**4.1 Determination of the IGCs:**

In the studied TPM of type PRRR-PRPU, the effects of all the geometric errors that do not violate its translational nature can be eliminated through calibration procedures. Therefore, the geometric constants whose errors do not affect the translational constraint between platform and base are assumed without relevant geometric errors. The analysis that identifies the IGCs in the base, the platform, and the two limbs is reported below.

The base geometry just fixes the angles among the two P-pair sliding directions. Since it is quite clear that the translational constraint between the platform and the base remains valid, even though these two directions are not orthogonal, the base geometry is assumed without geometric errors.

The platform geometry fixes only the minimum distance, $a_p$ [Fig. 1(c)], between two R-pair axes (one of the PRRR limb and the other of the PRPU limb). Any variation in this geometric datum just yields a constant change in the location of the $O_p$−$x_py_pz_p$ reference frame, fixed to the platform; such constant change does not affect the translational constraint between the platform and the base. Thus, the platform geometry is assumed without geometric errors.

Regarding the PRPU limb (see Fig.1), its static analysis reveals that the force system, it applies to the platform, is constituted by one torque perpendicular to the two R-pair axes of the U-joint and two forces, which are parallel to the sliding directions of the two actuated P pairs [i.e., one to the coordinate axis $x_b$ and the other to the line passing through the points $A_1$ and $B_1$ (Fig. 1(c))] and have both the lines of actions passing through point $A_1$. The translational constraint between platform and base only needs that the torque has a component along the coordinate

[11] $|s|$ and $||\mathbf{v}||$ denote the absolute value of the scalar s and the Euclidean norm of the vector $\mathbf{v}$, respectively; whereas, $\Delta(\cdot)$ denotes a small finite variation of $(\cdot)$.

axis $y_b$. Even though this condition is not altered by the links' geometric errors, a mobility analysis reveals that the parallelism of the axes of the two intermediate R-pairs, and the perpendicularity of the axes of the two R-pairs that form the U-joint are necessary to keep the translational constraint between platform and base. Therefore, it will be assumed that geometric errors are present only in the parallelism of the axes of the two intermediate R-pairs, and in the perpendicularity of the axes of the two R-pairs that form the U-joint. In so doing, the geometry of this limb is modified as shown in Fig. 10 where $d_2$, $d_3$, h, $\alpha_1$ and $\alpha_2$ are the geometric errors that become additional passive-joint variables of the ESM thus transforming the PRPU limb into a PRPRPRPRRP limb.

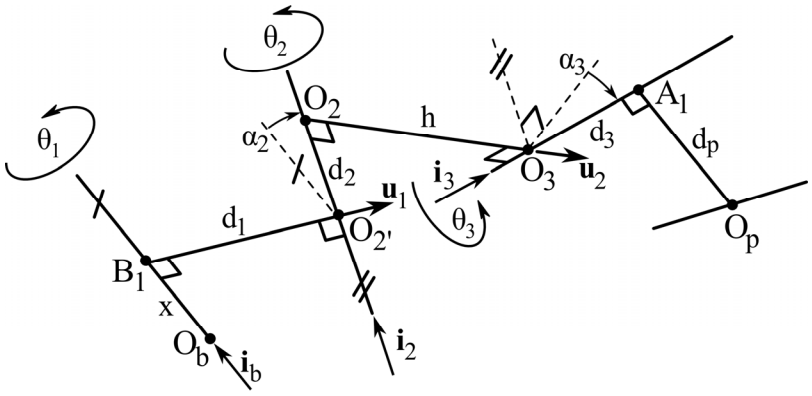


**Figure 10:** PRPU limb with geometric errors.

With reference to the Fig. 10, $\mathbf{i}_2$ and $\mathbf{i}_3$ are the axis unit vectors of the two R-pair that constitute U-joint, and the following relationships hold

$$\mathbf{i}_2 = \mathbf{i}_b \cos\alpha_2 + (\mathbf{u}_1 \times \mathbf{i}_b) \sin\alpha_2 \tag{23a}$$

$$\mathbf{i}_3 = -\mathbf{i}_2 \sin\alpha_3 + (\mathbf{u}_2 \times \mathbf{i}_2) \cos\alpha_3 \tag{23b}$$

$$d_2 = (\mathbf{O}_2 - \mathbf{O}_{2'}) \cdot \mathbf{i}_2 \tag{23c}$$

$$d_3 = (\mathbf{A}_1 - \mathbf{O}_3) \cdot \mathbf{i}_3 \tag{23d}$$

where $\mathbf{u}_1 = (\mathbf{O}_{2'} - \mathbf{B}_1)/d_1$ and $\mathbf{u}_2 = \mathbf{u}_1 \cos\theta_2 - (\mathbf{u}_1 \times \mathbf{i}_2) \sin\theta_2$. The PRPU limb with geometric errors (i.e., the above-mentioned PRPRPRPRRP limb of the ESM) makes it possible to write the platform twist $\$ [\equiv(\boldsymbol{\omega}^T, \dot{\mathbf{O}}_p^T)^T]$ as follows

$$\$ = \hat{\$}_x \dot{x} + \hat{\$}_d \dot{d}_1 + \sum_{j=1,3} \hat{\$}_j \dot{\theta}_j + \hat{\$}_h \dot{h} + \sum_{k=2,3} (\hat{\$}_{P,k} \dot{d}_k + \hat{\$}_{R,k} \dot{\alpha}_k) \tag{24}$$

where

$$\hat{\$}_x = \begin{bmatrix} \mathbf{0} \\ \mathbf{i}_b \end{bmatrix};\ \hat{\$}_d = \begin{bmatrix} \mathbf{0} \\ \mathbf{u}_1 \end{bmatrix};\ \hat{\$}_1 = \begin{bmatrix} \mathbf{i}_b \\ (\mathbf{B}_1 - \mathbf{O}_p) \times \mathbf{i}_b \end{bmatrix};\ \hat{\$}_2 = \begin{bmatrix} \mathbf{i}_2 \\ (\mathbf{O}_2 - \mathbf{O}_p) \times \mathbf{i}_2 \end{bmatrix};\ \hat{\$}_3 = \begin{bmatrix} \mathbf{i}_3 \\ (\mathbf{A}_1 - \mathbf{O}_p) \times \mathbf{i}_3 \end{bmatrix};$$

$$\hat{\$}_h = \begin{bmatrix} \mathbf{0} \\ \mathbf{u}_2 \end{bmatrix};\ \hat{\$}_{P,2} = \begin{bmatrix} \mathbf{0} \\ \mathbf{i}_2 \end{bmatrix};\ \hat{\$}_{P,3} = \begin{bmatrix} \mathbf{0} \\ \mathbf{i}_3 \end{bmatrix};\ \hat{\$}_{R,2} = \begin{bmatrix} \mathbf{u}_1 \\ (\mathbf{B}_1 - \mathbf{O}_p) \times \mathbf{u}_1 \end{bmatrix};\ \hat{\$}_{R,3} = \begin{bmatrix} \mathbf{u}_2 \\ (\mathbf{O}_2 - \mathbf{O}_p) \times \mathbf{u}_2 \end{bmatrix}.$$

Regarding the PRRR limb, a possible error in the parallelism between P-pair's sliding direction and the axis of the first R-pair or in the values of the lengths $a_1$ and $a_2$ does not change the type of motion it imposes to the platform (i.e., it still is a Shoenflies motion). On the contrary, a possible error in the parallelism among the three R-pair axes does change that motion and violates the translational constraint between the platform and the base. Therefore, it will be assumed that geometric errors are present only in the parallelism among the three R-pair axes. In so doing, the geometry of this limb is modified as shown in Fig. 11 where $d_4$, $d_5$, $\alpha_4$ and $\alpha_5$ are the geometric errors that become additional passive-joint variables of the ESM thus transforming the PRRR limb into a PRRPRRPR limb.

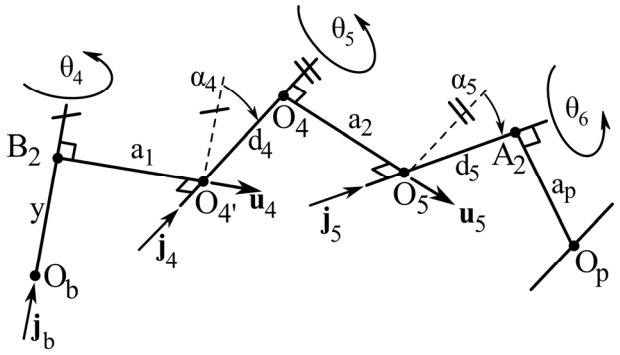


**Figure 11:** PRRR limb with geometric errors.

With reference to the Fig. 11, $\mathbf{j}_4$ and $\mathbf{j}_5$ are the unit vectors of the second and the third R-pair axes, respectively, and the following relationships hold

$$\begin{aligned} \mathbf{j}_4 &= \mathbf{j}_b \cos\alpha_4 + (\mathbf{u}_4 \times \mathbf{j}_b) \sin\alpha_4 \\ \mathbf{j}_5 &= \mathbf{j}_4 \cos\alpha_5 + (\mathbf{u}_5 \times \mathbf{j}_4) \sin\alpha_5 \\ d_4 &= (\mathbf{O}_4 - \mathbf{O}_{4'}) \cdot \mathbf{j}_4 \\ d_5 &= (\mathbf{A}_2 - \mathbf{O}_5) \cdot \mathbf{j}_5 \end{aligned} \tag{30}$$

where $\mathbf{u}_4 = (\mathbf{O}_{4'} - \mathbf{B}_2)/a_1$ and $\mathbf{u}_5 = (\mathbf{O}_5 - \mathbf{O}_4)/a_2$. Also, the PRRR limb with geometric errors (i.e., the above-mentioned PRRPRRPR limb of the ESM) makes it possible to write the platform twist $\$ [\equiv(\boldsymbol{\omega}^T, \dot{\mathbf{O}}_p^T)^T]$ as follows

$$\$ = \hat{\$}_y \dot{y} + \sum_{j=4,6} \hat{\$}_j \dot{\theta}_j + \sum_{k=4,5} (\hat{\$}_{P,k} \dot{d}_k + \hat{\$}_{R,k} \dot{\alpha}_k) \tag{31}$$

where

$$\hat{\$}_y=\begin{bmatrix}\mathbf{0}\\ \mathbf{j}_b\end{bmatrix};\ \hat{\$}_4=\begin{bmatrix}\mathbf{j}_b\\ (\mathbf{B}_2-\mathbf{O}_p)\times\mathbf{j}_b\end{bmatrix};\ \hat{\$}_5=\begin{bmatrix}\mathbf{j}_4\\ (\mathbf{O}_4-\mathbf{O}_p)\times\mathbf{j}_4\end{bmatrix};\ \hat{\$}_6=\begin{bmatrix}\mathbf{j}_5\\ (\mathbf{O}_5-\mathbf{O}_p)\times\mathbf{j}_5\end{bmatrix};$$

$$\hat{\$}_{P,4}=\begin{bmatrix}\mathbf{0}\\ \mathbf{j}_4\end{bmatrix};\ \hat{\$}_{P,5}=\begin{bmatrix}\mathbf{0}\\ \mathbf{j}_5\end{bmatrix};\ \hat{\$}_{R,4}=\begin{bmatrix}\mathbf{u}_4\\ (\mathbf{B}_2-\mathbf{O}_p)\times\mathbf{u}_4\end{bmatrix};\ \hat{\$}_{R,5}=\begin{bmatrix}\mathbf{u}_5\\ (\mathbf{O}_4-\mathbf{O}_p)\times\mathbf{u}_5\end{bmatrix}.$$

**4.2 ESM and Jacobian Matrices:**

Subsection 4.1 brings to conclude that the ESM is a PRRPRRPR-PRPRPRPRRP mechanism with $\mathbf{q}_{f,P}=(x,y,d_1)^T$, $\mathbf{q}_{f,R}=(0,0,0)^T$, $\mathbf{q}_{g,P}=(d_2, d_3, d_4, d_5, h)^T$, and $\mathbf{q}_{g,R}=(\alpha_2, \alpha_3, \alpha_4, \alpha_5)^T$. Also, the equation system constituted by Eqs. (24) and (31) can be transformed as follows after Eq. (24) is replaced by the subtraction of Eq. (31) from Eq. (24):

$$\$=\mathbf{A}_f\dot{\mathbf{q}}_{f,P}+\mathbf{A}_{(r\text{-}f)}\dot{\mathbf{q}}_{(r\text{-}f)}+\mathbf{A}_{g,P}\dot{\mathbf{q}}_{g,P}+\mathbf{A}_{g,R}\dot{\mathbf{q}}_{g,R} \tag{32a}$$

$$\mathbf{B}_{(r\text{-}f)}\dot{\mathbf{q}}_{(r\text{-}f)}=\mathbf{B}_f\dot{\mathbf{q}}_{f,P}+\mathbf{B}_{g,P}\dot{\mathbf{q}}_{g,P}+\mathbf{B}_{g,R}\dot{\mathbf{q}}_{g,R} \tag{32b}$$

where $\mathbf{q}_{(r\text{-}f)}=(\theta_1, \theta_2, \theta_3, \theta_4, \theta_5, \theta_6)^T$, and

$\mathbf{A}_f=\left[\mathbf{0},\hat{\$}_y,\mathbf{0}\right]$; $\mathbf{A}_{r\text{-}f}=\left[\mathbf{0},\mathbf{0},\mathbf{0},\hat{\$}_4,\hat{\$}_5,\hat{\$}_6\right]$; $\mathbf{A}_{g,P}=\left[\mathbf{0},\mathbf{0},\hat{\$}_{P,4},\hat{\$}_{P,5},\mathbf{0}\right]$; $\mathbf{A}_{g,R}=\left[\mathbf{0},\mathbf{0},\hat{\$}_{R,4},\hat{\$}_{R,5}\right]$;

$\mathbf{B}_f=\left[\hat{\$}_x,-\hat{\$}_y,\hat{\$}_d\right]$; $\mathbf{B}_{r\text{-}f}=\left[-\hat{\$}_1,-\hat{\$}_2,-\hat{\$}_3,\hat{\$}_4,\hat{\$}_5,\hat{\$}_6\right]$; $\mathbf{B}_{g,P}=\left[\hat{\$}_{P,2},\hat{\$}_{P,3},-\hat{\$}_{P,4},-\hat{\$}_{P,5},\hat{\$}_h\right]$;

$\mathbf{B}_{g,R}=\left[\hat{\$}_{R,2},\hat{\$}_{R,3},-\hat{\$}_{R,4},-\hat{\$}_{R,5}\right]$.

If Eq. (32b) is exploited to linearly eliminate $\dot{\mathbf{q}}_{(r\text{-}f)}$ from Eq. (32a), Eq. (32a) will become the sought-after instantaneous input-output relationship of the ESM, that is,

$$\boldsymbol{\omega}=\mathbf{D}_{f,P}\ \dot{\mathbf{q}}_{f,P}+\mathbf{D}_{g,P}\ \dot{\mathbf{q}}_{g,P}+\mathbf{D}_{g,R}\ \dot{\mathbf{q}}_{g,R} \tag{33a}$$

$$\dot{\mathbf{O}}_p=\mathbf{E}_{f,P}\ \dot{\mathbf{q}}_{f,P}+\mathbf{E}_{g,P}\ \dot{\mathbf{q}}_{g,P}+\mathbf{E}_{g,R}\ \dot{\mathbf{q}}_{g,R} \tag{33b}$$

where

$$\begin{bmatrix}\mathbf{D}_{f,P}\\ \mathbf{E}_{f,P}\end{bmatrix}=\mathbf{A}_f+\mathbf{A}_{(r\text{-}f)}\mathbf{B}_{(r\text{-}f)}^{-1}\mathbf{B}_f;\quad \begin{bmatrix}\mathbf{D}_{g,P}\\ \mathbf{E}_{g,P}\end{bmatrix}=\mathbf{A}_{g,P}+\mathbf{A}_{(r\text{-}f)}\mathbf{B}_{(r\text{-}f)}^{-1}\mathbf{B}_{g,P}\ ;\quad \begin{bmatrix}\mathbf{D}_{g,R}\\ \mathbf{E}_{g,R}\end{bmatrix}=\mathbf{A}_{g,R}+\mathbf{A}_{(r\text{-}f)}\mathbf{B}_{(r\text{-}f)}^{-1}\mathbf{B}_{g,R}$$

**4.3 Determination of the Accuracy Coefficients:**

In the nominal geometry (i.e., with reference to Figs. 1, 10 and 11, when $\mathbf{i}_2=\mathbf{i}_b$, $\mathbf{i}_3=\mathbf{k}_b$, $\mathbf{u}_2=\mathbf{j}_b$, $\mathbf{O}_{2'}\equiv\mathbf{O}_2\equiv\mathbf{O}_3\equiv\mathbf{A}_1$, $\mathbf{j}_4=\mathbf{j}_5=\mathbf{j}_b$, $\mathbf{O}_{4'}\equiv\mathbf{O}_4\equiv\mathbf{C}$ and $\mathbf{O}_5\equiv\mathbf{A}_2$), $\mathbf{D}_{f,P}$ and $\mathbf{D}_{g,P}$ are null matrices; whereas, $\mathbf{E}_{f,P}$ is equal to $\mathbf{H}^{-1}$, $\mathbf{D}_{g,R}$ is equal to $[\mathbf{v}_1, \mathbf{j}_b, \mathbf{u}_4, \mathbf{u}_5]$ with $\mathbf{v}_1=\mathbf{j}_b\cos\theta_1$, and

$$\mathbf{E}_{g,P}=\begin{bmatrix}1 & 0 & 0 & 0 & 0\\ 0 & 0 & 1 & 1 & 0\\ 0 & 1 & -\cot\theta_1 & -\cot\theta_1 & \cot\theta_1\end{bmatrix};$$

$$\mathbf{E}_{g,R}=\begin{bmatrix} 0 & 0 & d_p\sin\theta_4 & d_p\sin(\theta_4+\theta_5) \\ 0 & 0 & -d_1\sin\theta_1\cos\theta_4 - x\sin\theta_4 & -d_1\sin\theta_1\cos(\theta_4+\theta_5) - x\sin(\theta_4+\theta_5) + a_1\sin\theta_5 \\ 0 & 0 & y\cos\theta_4 + x\sin\theta_4\dfrac{\cos\theta_1}{\sin\theta_1} & y\cos(\theta_4+\theta_5) + x\sin(\theta_4+\theta_5)\dfrac{\cos\theta_1}{\sin\theta_1} - a_1\sin\theta_5\dfrac{\cos\theta_1}{\sin\theta_1} \end{bmatrix}.$$

The result is that $\delta_{f,P}$, $\delta_{f,R}$, $\delta_{g,P}$ and $\varepsilon_{f,R}$ are all equal to zero, and, for the studied TPM, inequalities (22a) and (22b) become

$$|\Delta\varphi| \le \delta_{g,R}\,||\Delta\mathbf{q}_{g,R}|| \tag{34a}$$

$$||\Delta\mathbf{O}_p|| \le \varepsilon_{f,P}\,||\Delta\mathbf{q}_{f,P}|| + \varepsilon_{g,P}\,||\Delta\mathbf{q}_{g,P}|| + \varepsilon_{g,R}\,||\Delta\mathbf{q}_{g,R}|| \tag{34b}$$

where $\delta_{g,R}$, $\varepsilon_{f,P}$, $\varepsilon_{g,P}$ and $\varepsilon_{g,R}$ are the largest singular values of the Jacobian matrices $\mathbf{D}_{g,R}$ , $\mathbf{E}_{f,P}$, $\mathbf{E}_{g,P}$ , and $\mathbf{E}_{g,R}$, respectively, with $\varepsilon_{f,P}$ and $\varepsilon_{g,P}$ that depend only on $\theta_1$ and have the following explicit expressions

$$\varepsilon_{f,P} = \sqrt{\frac{1}{1-|\cos\theta_1|}} \tag{35a}$$

$$\varepsilon_{g,P} = \sqrt{\frac{3+3\cot^2\theta_1+\sqrt{1+10\cot^2\theta_1+9\cot^4\theta_1}}{2}} \tag{35b}$$

The values of the accuracy coefficients $\delta_{g,R}$, $\varepsilon_{f,P}$, $\varepsilon_{g,P}$ and $\varepsilon_{g,R}$ depend on the TPM configuration. Figures 12 – 15 show their values on five planar sections of the useful workspace $V_u$. Also, their numerical evaluation inside $V_u$ reveals that they are bounded as follows

$$1 \le \delta_{g,R} \le 1.414075$$

$$1 \le \varepsilon_{f,P} \le 1.331184$$

$$\sqrt{2} \le \varepsilon_{g,P} \le 1.682512$$

$$0.169423 \le \varepsilon_{g,R} \le 0.743451 \text{ (l.u./rad)}$$

The introduction of their maximum values into inequalities (34a) and (34b) brings to conclude that, in $V_u$, the positioning precision of the studied TPM has the following upper bounds

$$|\Delta\varphi|_{max} = 1.414075\,||\Delta\mathbf{q}_{g,R}|| \tag{36a}$$

$$||\Delta\mathbf{O}_p||_{max} = 1.331184\,||\Delta\mathbf{q}_{f,P}|| + 1.682512\,||\Delta\mathbf{q}_{g,P}|| + 0.743451\,||\Delta\mathbf{q}_{g,R}|| \tag{36b}$$

If $|\Delta\varphi|_{max}$ is chosen equal to 0.026180 rad (=1.5°)[12], Eq. (36a) will give the following upper bound

$$||\Delta\mathbf{q}_{g,R}||_{max} = 0.018514 \text{ rad} \tag{37}$$

Since $||\Delta\mathbf{q}_{g,R}||$ is equal to $\sqrt{\alpha_2^2+\alpha_3^2+\alpha_4^2+\alpha_5^2}$ , if the choice of assigning the same tolerance class, $\alpha_T$, to all the angular errors $\alpha_2$, $\alpha_3$, $\alpha_4$, and $\alpha_5$ is adopted, Eq. (37) will give the following limitation on $\alpha_T$

$$\alpha_T \leq \frac{\left\|\Delta \mathbf{q}_{g,R}\right\|_{max}}{2} = 0.009257 \text{ rad} = 0.53° \tag{38}$$

Also, if $||\Delta \mathbf{q}_{g,P}||$ is assumed equal to 0.01(l.u.) and the joint-variable errors $\Delta x$, $\Delta y$, and $\Delta d_1$ are all assumed equal to 0.0001(l.u.)[13], $||\Delta \mathbf{q}_{f,P}||$ ($=\sqrt{(\Delta x)^2 + (\Delta y)^2 + (\Delta d_1)^2}$ ) will be equal to 0.0001732(l.u.) and inequality (36b) will give the following upper bound

$$||\Delta \mathbf{O}_p||_{max} = 0{,}031 \text{ (l.u.)} \tag{39}$$

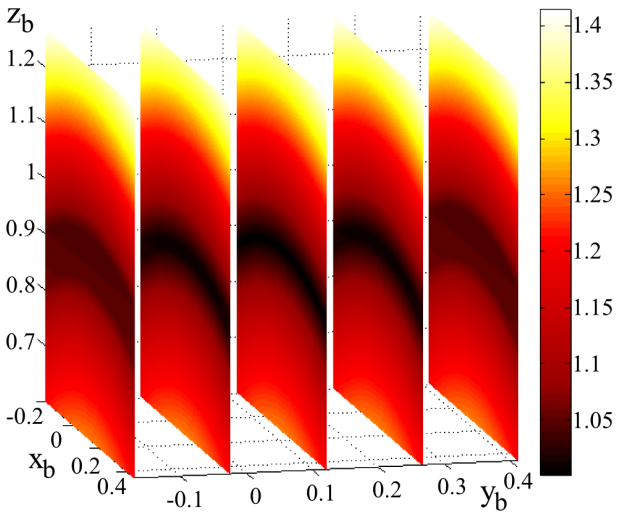


**Figure 12:** Values of $\delta_{g,R}$ inside the useful workspace.

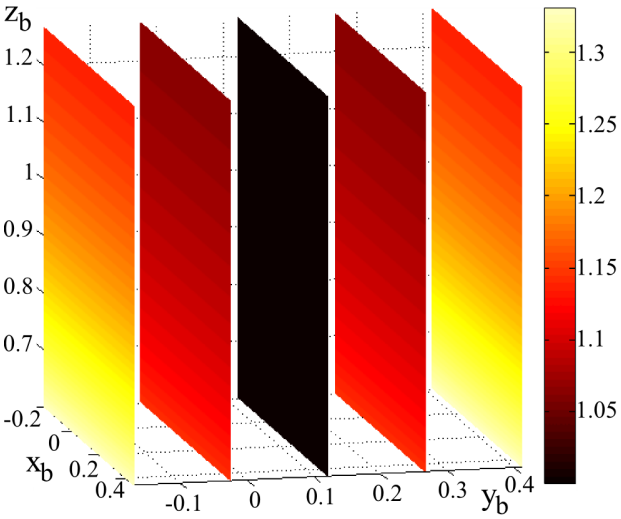


**Figure 13:** Values of $\varepsilon_{f,P}$ inside the useful workspace.

[12] This value of $|\Delta\varphi|_{max}$ has been taken from the data sheets of the commercial delta robot ABB IRB-360 (http://new.abb.com/products/robotics/industrial-robots/irb-360).

[13] It is worth noting that the data sheets of commercial roller-screws (see, for instance, http://www.thomsonlinear.com/website/com/eng/index.php or http://www.skf.com/group/products/linear-motion/ball-and-roller-screws/roller-screws/index.html ) give $\Delta d$=1μm.

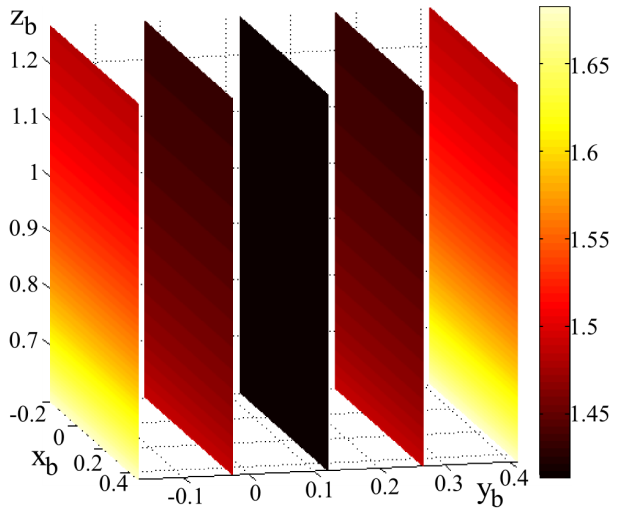


**Figure 14:** Values of $\varepsilon_{g,P}$ inside the useful workspace.

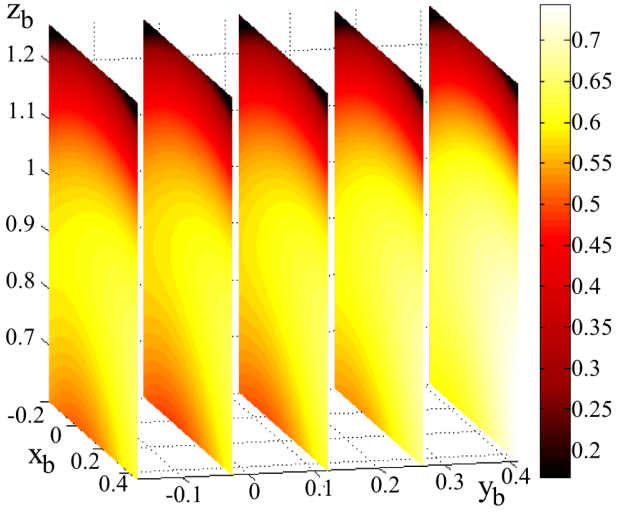


**Figure 15:** Values of $\varepsilon_{g,R}$ (l.u./rad) inside the useful workspace.

## 5. Conclusions

A method for the dimensional synthesis of any translational parallel manipulator (TPM) has been presented and adopted for the dimensional synthesis of the TPMs of type PRRR-PRPU that have been recently proposed by one of the authors. As far as these authors are aware the presented method is overall novel. It consists in a) the assignment of a small set of normalized dimensional data according to general criteria that produce a well-proportioned manipulator, b) the determination of the workspace regions that satisfy given design requirements on kinetostatics performances, c) the computation of the remaining dimensional data by maximizing the ratio (volumetric ratio) between the volumes of the useful workspace and of the TPM overall size, d) the stiffness analysis and e) the accuracy analysis.

The dimensional synthesis of TPMs of type PRRR-PRPU has been addressed for the first time. Addressing this design step on such TPMs is important since they have a number of promising features: a single-loop not-overconstrained architecture with all the actuators on or near to the base, a simple position analysis, easy-to-find workspace boundaries, no constraint singularity, a type-II singularity locus that is a plane easy to keep far from the useful workspace, and a double infinity of isotropic configurations.

This dimensional synthesis has brought to find a normalized TPM of type PRRR-PRPU, which yields a set of actual TPMs with the same performances by changing the actual value of the reference geometric length, named length unit (l.u.). The performances of all these TPMs are comparable with those of commercial TPMs. In particular, they have comparable kinetostatics performances ($CI_{min}$=0.63, GCI=0.855), volumetric ratio ($r_V$=0.266), stiffness and accuracy. Eventually, the chosen shape of the useful workspace (i.e., a cuboid) matches the needs of many industrial applications.

## Acknowledgments

This work has been developed at the Laboratory of Advanced Mechanics (MECH-LAV) of Ferrara Technopole, supported by UNIFE-FIR2016 funds, by Regione Emilia Romagna (District Councillorship for Productive Assets, Economic Development, Telematic Plan) POR-FESR 2007-2013, Attività I.1.1, and by CNPq – Conselho Nacional de Desenvolvimento Científico e Tecnológico (National Council for Scientific and Technological Development) -Project nº 232250/2014-6 - Brazil.

## References

1. X. Kong, C. M. Gosselin, ‘‘Type Synthesis of Parallel Mechanisms,’’, Springer-Verlag, Berlin Heidelberg, Germany, 2007, ISBN: 978-3-540-71989-2.
2. J.M. Hervé, F. Sparacino, “Structural Synthesis of Parallel Robots Generating Spatial Translation,” *Proceedings of the 5th IEEE Int. Conf. on Advanced Robotics*, pp. 808–813, 1991.
3. G. Gogu, “Structural Synthesis of Parallel Robots: Part 2: Translational Topologies with Two and Three Degrees of Freedom,” Springer Netherlands, 2009, ISBN 978-1-4020-9793-5.
4. J.P. Merlet, “Parallel Robots,” Springer Netherlands, 2006, ISBN 978-1-4020-4132-7.
5. R. Di Gregorio, “Translational parallel manipulators: new proposals, Journal of Robotic Systems, 19 (12) (2002), pp. 595-603.
6. B. Li, Y. M. Li, X. H. Zhao,W. M. Ge, “Kinematic analysis of a novel 3-CRU translational parallel mechanism,” Mechanical Sciences, 6 (1) (2015), pp. 57-64.

7. J.K. Davidson, K.H. Hunt, “Robots and Screw Theory: applications of kinematics and statics to robotics,” Oxford University Press, New York (USA), 2004.
8. C.-C. Lee, J.M. Hervé, “Type synthesis of primitive Schoenflies-motion generators,” Mechanism and Machine Theory, 44 (2009), pp. 1980–1997
9. C.-C. Lee, J.M. Hervé, “On some applications of primitive Schönflies-motion generators,” Mechanism and Machine Theory, 44 (2009), pp. 2153–2163
10. J. Angeles, “Rational Kinematics,” Springer-Verlag, Inc., New York (USA), 1988.
11. R. Di Gregorio, “Kinematic analysis of a single-loop translational manipulator,” in: *ROMANSY 21- Robot Design, Dynamics and Control*, V.Parenti-Castelli and W. Schiehlen (eds.), Springer, New York (USA), pp. 73-79, 2016.
12. D. Zlatanov, I.A. Bonev, C.M. Gosselin, “Constraint singularities of parallel mechanisms,” *Proceedings of the 2002 IEEE International Conference on Robotics 8 Automation*, 2002, Washington, DC, pp. 496-502.
13. C. Gosselin and J. Angeles, "Singularity analysis of closed-loop kinematic chains," *IEEE Transactions on Robotics and Automation* **6** (3) 281-290 (1990).
14. O. Ma and J. Angeles, “Architecture singularities of platform manipulators,” *Proc. of the 1991 IEEE Int. Conf. on Robotics and Automation*, Sacramento (CA, USA), pp. 1542-1547 (1991).
15. D. Zlatanov, R.G. Fenton and B. Benhabib, “A unifying framework for classification and interpretation of mechanism singularities,” *ASME J. of Mechanical Design*, **117** (4) 566–572 (1995).
16. C. Gosselin, J. Angeles, “A global performance index for the kinematic optimization of robotic manipulators,” Journal of Mechanical Design, 113 (3), 1991, pp. 220-226
17. J. Angeles, C.S. Lòpez-Cajùn, C.S., “Kinematic Isotropy and the Conditioning Index of Serial Robotic Manipulators,” The International Journal of Robotics Research, 11 (6), 1992, pp. 560-571
18. Z. Li, Y. Lou, Y. Zhang, B. Liao, Z. Li, “Type Synthesis, Kinematic Analysis, and Optimal Design of a Novel Class of Schönflies-Motion Parallel Manipulators,” IEEE Transactions on Automation Science and Engineering, 10 (3), 2013, pp. 674–686.
19. Y. Lou, G. Liu, N. Chen, Z. Li, “Optimal design of parallel manipulators for maximum effective regular workspace,” Proceedings of the 2005 IEEE/RSJ Int. Conf. on Intelligent Robots and Systems, Edmonton, Canada, 2005, pp. 795–800.
20. S. Kucuk, Z. Bingul, “Comparative study of performance indices for fundamental robot manipulators,” Robotics and Autonomous Systems, 54 (7), 2006, pp. 567-573.

21. C. Gosselin, “Stiffness mapping for parallel manipulators,” IEEE Trans. Robot. Autom., 6(3), 1990, pp. 377–382.
22. H. Liu, T.T. Huang, D.G Chetwynd, “A general approach for geometric error modeling of lower mobility parallel manipulators,” ASME Journal of Mechanisms and Robotics, 3(2), 2011, pp. 021013-(1:13).
23. H. Simas, R. Di Gregorio, “Geometric Error Effects on Manipulators’ Positioning Precision: A General Analysis and Evaluation Method,” ASME Journal of Mechanisms and Robotics, 8(6), 2016, pp. 061016-(1:10).
24. J.-P. Merlet, “Optimal Design of Robots,” Proceedings of Robotics: Science and Systems I, 2005, Boston (USA), pp. 311-318.
25. J.-P. Merlet J-P., “Jacobian, Manipulability, Condition Number, and Accuracy of Parallel Robots,” ASME J. Mech. Des.,128(1), 2006, pp. 199-206.
26. X.-J. Liu, J. Wang, J., “Parallel kinematics: type, kinematics, and optimal design,” Springer, New York (USA), 2014.
27. M. Wu, D. Zhang, X. Zhao, “Conceptual Design and Kinematic Performance Evaluation of a New Asymmetrical Parallel Robot,” Proc. of the IEEE 2007 International Conference on Mechatronics and Automation, Harbin (China), 2007, pp. 2854–2859.
28. Y. Li, Q. Xu, “Kinematics and Dexterity Analysis for a Novel 3-DOF Translational Parallel Manipulator,” Proceedings of the 2005 IEEE International Conference on Robotics and Automation, 2005, Barcelona (Spain), pp. 2944–2949.
29. C. D. Meyer, “Matrix Analysis and Applied Linear Algebra,” Society for Industrial & Applied Mathematics (SIAM), 2000.
30. Y. Lou, G. Liu, N. Chen, Z. Li, “Optimal design of parallel manipulators for maximum effective regular workspace,” Proceedings of the 2005 IEEE/RSJ Int. Conf. on Intelligent Robots and Systems, Edmonton, Canada, 2005, pp. 795–800.
31. J. Wang, X. Liu, C. Wu, “Optimal design of a new spatial 3-DOF parallel robot with respect to a frame-free index,” Science in China Series E: Technological Sciences, 52 (4), 2009, pp. 986–999.
32. R.S. Hartenberg, J. Denavit, “Kinematic Synthesis of Linkages,” McGraw-Hill, New York (USA), 1964.
33. L.-W. Tsai, “Robot Analysis: The Mechanics of Serial and Parallel Manipulators,” John Wiley & Sons, New York (USA), 1999.
34. G. Legnani, I. Fassi, H. Giberti, S. Cinquemani, D. Tosi, “A new isotropic and decoupled 6-DoF parallel manipulator,” Mechanism and Machine Theory, 58 (1), 2012, pp. 64–81 (2012).

35. A. Pashkevich, D. Chablat, P. Wenger, “Stiffness analysis of overconstrained parallel manipulators,” Mechanism and Machine Theory, 44 (2009), pp. 966–982.

36. R. Di Gregorio, V. Parenti-Castelli, “Geometric Errors Versus Calibration in Manipulators with Less than 6 DOF,” RoManSy 14 – Theory and practice of robots and manipulators, Bianchi G., Guinot J.-C. and Rzymkowski C. (eds.), Springer, New York, 2002, pp. 31-38.